ANALYTICAL PERFORMANCE ASSESSMENT OF ESPRIT-TYPE ALGORITHMS FOR COEXISTING CIRCULAR AND STRICTLY NON-CIRCULAR SIGNALS

Jens Steinwandt [1], *Florian Roemer* [2,3], *and Martin Haardt* [1]

[1] Communications Research Laboratory, Ilmenau University of Technology, P.O. Box 100565, 98684 Ilmenau, Germany
[2] Digital Broadcasting Research Laboratory, Ilmenau University of Technology, P.O. Box 100565, 98684 Ilmenau, Germany
[3] Fraunhofer Institute for Integrated Circuits IIS
{jens.steinwandt, florian.roemer, martin.haardt}@tu-ilmenau.de, www.tu-ilmenau.de/crl

ABSTRACT

Estimating the directions of arrival (DOA) of coexisting circular and strictly second-order (SO) non-circular (NC) signals has recently emerged as an active field of research. In previous work, we have proposed two ESPRIT-type algorithms, i.e., C-NC Standard ESPRIT and C-NC Unitary ESPRIT, for this scenario that improve the estimation accuracy of the conventional schemes and increase the number of resolvable signals. In this paper, we present a first-order performance assessment of these two ESPRIT-type algorithms. Specifically, we derive closed-form mean square error (MSE) expressions that are asymptotic in the effective signal-to-noise ratio (SNR), i.e., the approximations become exact for either high SNRs or a large sample size. Apart from a zero mean and finite SO moments, no further assumptions on the noise statistics are required. We show that both algorithms perform identical in the high effective SNR regime. Moreover, the analytical results verify the previously observed property that the presence of strictly non-circular sources improves the estimation accuracy of the circular signals.

Index Terms— ESPRIT, non-circular sources, mixture, DOA estimation.

1. INTRODUCTION

High resolution direction of arrival (DOA) estimation has long been a fundamental research area in the field of array signal processing. Such a task arises in a wide range of applications including radar, sonar, channel sounding, and wireless communications. In some of these applications, the received signals exhibit a strictly second-order (SO) non-circular (NC) structure [1]. Examples of digital modulation schemes that use such signals are BPSK, PAM, Offset-QPSK, ASK, etc. Previous work has shown that taking advantage of the strict non-circularity of the impinging signals helps to improve the performance of traditional parameter estimation algorithms. This observation has sparked the development of a number of improved subspace-based parameter estimation schemes such as NC MUSIC [2], NC Root-MUSIC [3], NC Standard ESPRIT [4], and NC Unitary ESPRIT [5], [6]. It has been reported that these methods efficiently exploit the prior knowledge of the signals' strict non-circularity, thus providing a significant improvement in the estimation accuracy and doubling the number of resolvable sources [6].

The observed benefits associated with NC sources have raised a considerable research interest in the analytical performance evaluation of the NC DOA algorithms in order to quantify the achievable improvements objectively. As a result, the performance of NC MUSIC as well as NC Standard ESPRIT and NC Unitary ESPRIT has been investigated in [2], [6], and [7]. One of the most prominent performance assessment concepts in [8] along with [9], which provides the basis for the studies in [6], yields an explicit first-order approximation of the estimation error caused by the perturbed subspace estimate due to a small noise contribution. It is asymptotic in the effective signal-to-noise ratio (SNR), i.e., the expressions become exact for either high SNRs or a large sample size. Moreover, for the resulting mean square error (MSE) expressions, no further assumptions on the noise statistics apart from a zero mean and finite SO moments are required. This analysis allows to explicitly assess the achievable asymptotic performance of the NC algorithms.

However, as the mentioned NC algorithms rest on the assumption that all the signals are strictly non-circular, they cannot handle the more general case of coexisting circular and strictly non-circular signals. In recent years, several parameter estimation schemes based on spectral MUSIC [10]-[12] and ESPRIT [13] have been proposed for this mixed signal scenario. The latter is particularly appealing as it provides closed-form estimates while requiring a low complexity. It was shown that the methods [10]-[13] perform better than the non-NC schemes and simultaneously increase the number of resolvable signals. Inspired by [14], a deterministic Cramér-Rao bound has been developed in [15] as a benchmark for the mixed signal scenario. However, an analytical performance assessment of the algorithms has not been reported in the literature to date.

In this paper, we present a performance analysis of the 1-D C-NC Standard/Unitary ESPRIT algorithms [13] for coexisting circular and strictly non-circular signals. For both algorithms, least squares (LS) is used to solve the shift-invariance equations. We derive closed-form first-order expansions for the estimation error in terms of the noise realization and generic MSE expressions based on the concepts from [8] and [9]. Similarly to the NC signal only case, it is shown that C-NC Standard ESPRIT and C-NC Unitary ESPRIT perform identically in the high effective SNR regime. Moreover, by numerical evaluation of the analytical expressions, we verify the previously observed property that the presence of NC sources improves the estimation accuracy of the circular sources.

2. DATA MODEL

Suppose that d planar wavefronts emitted by narrowband sources in the far field are received by a shift-invariant-structured array composed of M identical elements. The observations at N snapshots are collected in the measurement matrix

$$\boldsymbol{X} = \boldsymbol{A}\boldsymbol{S} + \boldsymbol{N} \in \mathbb{C}^{M \times N}, \tag{1}$$

where the array steering matrix $\boldsymbol{A} = [\boldsymbol{a}(\mu_1), \ldots, \boldsymbol{a}(\mu_d)] \in \mathbb{C}^{M \times d}$ consists of the array steering vectors $\boldsymbol{a}(\mu_i)$ corresponding to the i-th

This work was supported by the DFG project EXPRESS (HA 2239/6-1).

spatial frequency $\mu_i,\ i=1,\ldots,d$. Moreover, $\boldsymbol{S}\in\mathbb{C}^{d\times N}$ is the symbol matrix and $\boldsymbol{N}\in\mathbb{C}^{M\times N}$ represents the additive zero-mean sensor noise.

In order to model the mixture of strictly non-circular and circular signals, we partition $\boldsymbol{S}$ into $\boldsymbol{S}=[\boldsymbol{S}_{\mathrm{nc}}^{\mathrm{T}},\boldsymbol{S}_{\mathrm{c}}^{\mathrm{T}}]^{\mathrm{T}}$. Thus, $\boldsymbol{S}_{\mathrm{nc}}\in\mathbb{C}^{d^{(\mathrm{nc})}\times N}$ and $\boldsymbol{S}_{\mathrm{c}}\in\mathbb{C}^{d^{(\mathrm{c})}\times N}$ represent the symbol matrices of the $d^{(\mathrm{nc})}$ strictly non-circular and the $d^{(\mathrm{c})}$ circular signals, respectively, such that $d^{(\mathrm{nc})}+d^{(\mathrm{c})}=d$. Then, we virtually decompose each of the circular sources into two strictly non-circular sources with the same DOA [13]. Therefore, the symbol matrix $\boldsymbol{S}$ can be written as

$$\boldsymbol{S}=\begin{bmatrix}\boldsymbol{\Psi}^{(\mathrm{nc})} & \boldsymbol{0}\\ \boldsymbol{0} & \begin{bmatrix}\boldsymbol{I}_{d^{(\mathrm{c})}} & \mathrm{j}\boldsymbol{I}_{d^{(\mathrm{c})}}\end{bmatrix}\end{bmatrix}\begin{bmatrix}\boldsymbol{S}_0\\ \boldsymbol{S}_{\mathrm{R}}\\ \boldsymbol{S}_{\mathrm{I}}\end{bmatrix}=\boldsymbol{\Psi}\tilde{\boldsymbol{S}},\qquad(2)$$

where $\boldsymbol{\Psi}^{(\mathrm{nc})}=\mathrm{diag}\{\mathrm{e}^{\mathrm{j}\varphi_k}\}_{k=1}^{d^{(\mathrm{nc})}}$ represents the rotation phases corresponding to the strictly non-circular and circular sources, respectively. Additionally, we have $\boldsymbol{\Psi}\in\mathbb{C}^{d\times\tilde{d}}$ with $\tilde{d}=d^{(\mathrm{nc})}+2d^{(\mathrm{c})}$ and the real-valued matrix $\tilde{\boldsymbol{S}}\in\mathbb{R}^{\tilde{d}\times N}$ contains the symbols of the strictly non-circular sources $\boldsymbol{S}_0\in\mathbb{R}^{d^{(\mathrm{nc})}\times N}$ as well as the real and imaginary parts $\boldsymbol{S}_{\mathrm{R}}\in\mathbb{R}^{d^{(\mathrm{c})}\times N}$ and $\boldsymbol{S}_{\mathrm{I}}\in\mathbb{R}^{d^{(\mathrm{c})}\times N}$ of the circular signals, respectively.

Inserting (2) into (1) and splitting $\boldsymbol{A}=[\boldsymbol{A}_{\mathrm{nc}},\boldsymbol{A}_{\mathrm{c}}]$ with $\boldsymbol{A}_{\mathrm{nc}}\in\mathbb{C}^{M\times d^{(\mathrm{nc})}}$ and $\boldsymbol{A}_{\mathrm{c}}\in\mathbb{C}^{M\times d^{(\mathrm{c})}}$, the model in (1) can be expressed as

$$\boldsymbol{X}=\tilde{\boldsymbol{A}}\tilde{\boldsymbol{S}}+\boldsymbol{N},\qquad(3)$$

where $\tilde{\boldsymbol{A}}=\boldsymbol{A}\boldsymbol{\Psi}\in\mathbb{C}^{M\times\tilde{d}}$ is the modified array steering matrix. The new column dimensions of $\tilde{\boldsymbol{A}}$ again indicate the virtual decomposition of the circular sources into pairs of non-circular sources.

Applying ESPRIT-type algorithms, we require $\boldsymbol{A}$ to be shift-invariant, i.e., $\boldsymbol{J}_1\boldsymbol{A}\boldsymbol{\Phi}=\boldsymbol{J}_2\boldsymbol{A}$, where $\boldsymbol{J}_1,\boldsymbol{J}_2\in\mathbb{R}^{M^{(\mathrm{sel})}\times M}$ are the selection matrices and $\boldsymbol{\Phi}=\mathrm{diag}\{\mathrm{e}^{\mathrm{j}\mu_i}\}_{i=1}^{d}\in\mathbb{C}^{d\times d}$ contains the desired spatial frequencies. It is straightforward to see that in this case, $\tilde{\boldsymbol{A}}$ is also shift-invariant so that $\boldsymbol{J}_1\tilde{\boldsymbol{A}}\boldsymbol{\Gamma}=\boldsymbol{J}_2\tilde{\boldsymbol{A}}$, where the diagonal matrix $\boldsymbol{\Gamma}\in\mathbb{C}^{\tilde{d}\times\tilde{d}}$ contains the $\tilde{d}$ spatial frequencies.

3. REVIEW OF C-NC STANDARD ESPRIT

In order to take advantage of the strict non-circularity of the $d^{(\mathrm{nc})}$ sources, we apply the following preprocessing scheme to (3) by defining the augmented measurement matrix $\boldsymbol{X}^{(\mathrm{nc})}\in\mathbb{C}^{2M\times N}$ similarly to [5], [6] as

$$\boldsymbol{X}^{(\mathrm{nc})}=\begin{bmatrix}\boldsymbol{X}\\ \boldsymbol{\Pi}_M\boldsymbol{X}^*\end{bmatrix}=\begin{bmatrix}\tilde{\boldsymbol{A}}\\ \boldsymbol{\Pi}_M\tilde{\boldsymbol{A}}^*\end{bmatrix}\tilde{\boldsymbol{S}}+\begin{bmatrix}\boldsymbol{N}\\ \boldsymbol{\Pi}_M\boldsymbol{N}^*\end{bmatrix}\qquad(4)$$

$$=\boldsymbol{A}^{(\mathrm{nc})}\tilde{\boldsymbol{S}}+\boldsymbol{N}^{(\mathrm{nc})}=\boldsymbol{X}_0^{(\mathrm{nc})}+\boldsymbol{N}^{(\mathrm{nc})},\qquad(5)$$

where $\boldsymbol{\Pi}_M$ is the $M\times M$ exchange matrix with ones on its antidiagonal and zeros elsewhere, $\boldsymbol{A}^{(\mathrm{nc})}\in\mathbb{C}^{2M\times\tilde{d}}$ is the virtual steering matrix, and $\boldsymbol{X}_0^{(\mathrm{nc})}\in\mathbb{C}^{2M\times N}$ is the noise-free augmented measurement matrix. It can then be shown that the augmented array steering matrix $\boldsymbol{A}^{(\mathrm{nc})}$ also possesses the shift-invariance structure, i.e.,

$$\boldsymbol{J}_1^{(\mathrm{nc})}\boldsymbol{A}^{(\mathrm{nc})}\boldsymbol{\Gamma}=\boldsymbol{J}_2^{(\mathrm{nc})}\boldsymbol{A}^{(\mathrm{nc})},\qquad(6)$$

where the selection matrices $\boldsymbol{J}_1^{(\mathrm{nc})},\boldsymbol{J}_2^{(\mathrm{nc})}\in\mathbb{R}^{2M^{(\mathrm{sel})}\times 2M}$ are defined by

$$\boldsymbol{J}_1^{(\mathrm{nc})}=\begin{bmatrix}\boldsymbol{J}_1 & \boldsymbol{0}\\ \boldsymbol{0} & \boldsymbol{\Pi}_M^{(\mathrm{sel})}\boldsymbol{J}_2\boldsymbol{\Pi}_M\end{bmatrix},\ \boldsymbol{J}_2^{(\mathrm{nc})}=\begin{bmatrix}\boldsymbol{J}_2 & \boldsymbol{0}\\ \boldsymbol{0} & \boldsymbol{\Pi}_M^{(\mathrm{sel})}\boldsymbol{J}_1\boldsymbol{\Pi}_M\end{bmatrix}.$$

As $\boldsymbol{A}^{(\mathrm{nc})}$ is unknown, the augmented signal subspace $\hat{\boldsymbol{U}}_{\mathrm{s}}^{(\mathrm{nc})}\in\mathbb{C}^{2M\times\tilde{d}}$ is often estimated by computing the $\tilde{d}$ dominant left singular vectors from the augmented measurement matrix $\boldsymbol{X}^{(\mathrm{nc})}$ in (5). Then, a non-singular matrix $\boldsymbol{T}\in\mathbb{C}^{\tilde{d}\times\tilde{d}}$ can be found such that $\boldsymbol{A}^{(\mathrm{nc})}\approx\hat{\boldsymbol{U}}_{\mathrm{s}}^{(\mathrm{nc})}\boldsymbol{T}$. Using this relation, the augmented shift invariance equation is rewritten as

$$\boldsymbol{J}_1^{(\mathrm{nc})}\hat{\boldsymbol{U}}_{\mathrm{s}}^{(\mathrm{nc})}\boldsymbol{\Upsilon}\approx\boldsymbol{J}_2^{(\mathrm{nc})}\hat{\boldsymbol{U}}_{\mathrm{s}}^{(\mathrm{nc})},\qquad(7)$$

where $\boldsymbol{\Upsilon}\approx\boldsymbol{T}\boldsymbol{\Gamma}\boldsymbol{T}^{-1}$. Equation (7) can be solved for the unknown matrix $\boldsymbol{\Upsilon}\in\mathbb{C}^{\tilde{d}\times\tilde{d}}$ using least squares (LS), i.e.,

$$\hat{\boldsymbol{\Upsilon}}=\left(\boldsymbol{J}_1^{(\mathrm{nc})}\hat{\boldsymbol{U}}_{\mathrm{s}}^{(\mathrm{nc})}\right)^+\boldsymbol{J}_2^{(\mathrm{nc})}\hat{\boldsymbol{U}}_{\mathrm{s}}^{(\mathrm{nc})},\qquad(8)$$

where $(\cdot)^+$ denotes the Moore-Penrose pseudo inverse. Finally, the desired $\tilde{d}$ spatial frequency estimates are extracted via $\hat{\mu}_n=\arg\{\hat{\lambda}_n\},\ n=1,\ldots,\tilde{d}$, where $\hat{\lambda}_i$ are the eigenvalues of $\hat{\boldsymbol{\Upsilon}}$.

As we obtain $\tilde{d}=d^{(\mathrm{nc})}+2d^{(\mathrm{c})}$ instead of $d=d^{(\mathrm{nc})}+d^{(\mathrm{c})}$ spatial frequency estimates due to the decomposition in (2), we have proposed in [13] to combine the two correctly paired estimates for each circular source by averaging them according to

$$\hat{\mu}_\ell=\frac{1}{2}\left(\hat{\mu}_\ell^{(1)}+\hat{\mu}_\ell^{(2)}\right),\quad \ell=1,\ldots,d^{(\mathrm{c})}.\qquad(9)$$

Assuming $d^{(\mathrm{nc})}$ and $d^{(\mathrm{c})}$ known, the two estimates for each circular source can be identified by taking the $d^{(\mathrm{c})}$ pairs among all the estimates that are closest to each other.

4. PERFORMANCE OF C-NC STANDARD ESPRIT

For the performance analysis, we adopt the analytical framework proposed in [6], which is based on [8], [9]. Therein, an explicit first-order estimation error approximation is derived assuming that the noise-free signal is superimposed by a small additive noise perturbation, which is zero-mean with finite SO moments. As the structure of $\boldsymbol{X}^{(\mathrm{nc})}$ in (5) after the preprocessing scheme for non-circular sources is very similar to that in [6], the development for the analytical expressions from [6] is also applicable to the model in (5).

We first derive the signal subspace estimation error due to the small additive perturbation $\boldsymbol{N}^{(\mathrm{nc})}$. To this end, we consider $\boldsymbol{X}_0^{(\mathrm{nc})}$ and extract its noise-free subspaces as

$$\boldsymbol{X}_0^{(\mathrm{nc})}=\begin{bmatrix}\boldsymbol{U}_{\mathrm{s}}^{(\mathrm{nc})} & \boldsymbol{U}_{\mathrm{n}}^{(\mathrm{nc})}\end{bmatrix}\begin{bmatrix}\boldsymbol{\Sigma}_{\mathrm{s}}^{(\mathrm{nc})} & \boldsymbol{0}\\ \boldsymbol{0} & \boldsymbol{0}\end{bmatrix}\begin{bmatrix}\boldsymbol{V}_{\mathrm{s}}^{(\mathrm{nc})} & \boldsymbol{V}_{\mathrm{n}}^{(\mathrm{nc})}\end{bmatrix}^{\mathrm{H}},\qquad(10)$$

where $\boldsymbol{U}_{\mathrm{s}}^{(\mathrm{nc})}\in\mathbb{C}^{2M\times\tilde{d}}$, $\boldsymbol{U}_{\mathrm{n}}^{(\mathrm{nc})}\in\mathbb{C}^{2M\times(2M-\tilde{d})}$, and $\boldsymbol{V}_{\mathrm{s}}^{(\mathrm{nc})}\in\mathbb{C}^{N\times\tilde{d}}$ span the signal subspace, the noise subspace, and the row space, respectively. Moreover, $\boldsymbol{\Sigma}_{\mathrm{s}}^{(\mathrm{nc})}\in\mathbb{R}^{\tilde{d}\times\tilde{d}}$ contains the non-zero singular values on its diagonal. Writing the estimated signal subspace as $\hat{\boldsymbol{U}}_{\mathrm{s}}^{(\mathrm{nc})}=\boldsymbol{U}_{\mathrm{s}}^{(\mathrm{nc})}+\Delta\boldsymbol{U}_{\mathrm{s}}^{(\mathrm{nc})}$, where $\Delta\boldsymbol{U}_{\mathrm{s}}^{(\mathrm{nc})}$ denotes the subspace estimation error, we get the first-order approximation [6]

$$\Delta\boldsymbol{U}_{\mathrm{s}}^{(\mathrm{nc})}=\boldsymbol{U}_{\mathrm{n}}^{(\mathrm{nc})}\boldsymbol{U}_{\mathrm{n}}^{(\mathrm{nc})^{\mathrm{H}}}\boldsymbol{N}^{(\mathrm{nc})}\boldsymbol{V}_{\mathrm{s}}^{(\mathrm{nc})}\boldsymbol{\Sigma}_{\mathrm{s}}^{(\mathrm{nc})^{-1}}+\mathcal{O}\{\Delta^2\},\qquad(11)$$

where $\Delta=\|\boldsymbol{N}^{(\mathrm{nc})}\|$, and $\|\cdot\|$ represents a submultiplicative norm.

Then, the first-order approximation for the parameter estimation error $\Delta\mu_i=\hat{\mu}_i-\mu_i$ of C-NC Standard ESPRIT for the i-th spatial frequency can be written as

$$\Delta\mu_i=\mathrm{Im}\left\{\boldsymbol{p}_i^{\mathrm{T}}\left(\boldsymbol{J}_1^{(\mathrm{nc})}\boldsymbol{U}_{\mathrm{s}}^{(\mathrm{nc})}\right)^+\left[\boldsymbol{J}_2^{(\mathrm{nc})}/\lambda_i-\boldsymbol{J}_1^{(\mathrm{nc})}\right]\Delta\boldsymbol{U}_{\mathrm{s}}^{(\mathrm{nc})}\boldsymbol{q}_i\right\}+\mathcal{O}\{\Delta^2\},\qquad(12)$$

where $\lambda_i = \mathrm{e}^{\mathrm{j}\mu_i}$ is the i-th eigenvalue of $\boldsymbol{\Upsilon}$, $\boldsymbol{q}_i$ represents the i-th eigenvector of $\boldsymbol{\Upsilon}$ and the i-th column vector of the eigenvector matrix $\boldsymbol{Q}$, and $\boldsymbol{p}_i^{\mathrm{T}}$ is the i-th row vector of $\boldsymbol{P} = \boldsymbol{Q}^{-1}$. Hence, the eigendecomposition of $\boldsymbol{\Upsilon}$ is given by $\boldsymbol{\Upsilon} = \boldsymbol{Q}\boldsymbol{\Lambda}\boldsymbol{Q}^{-1}$, where $\boldsymbol{\Lambda}$ contains the eigenvalues λ_i on its diagonal. Inserting (11) into (12), we can write (12) explicitly in terms of the noise perturbation $\boldsymbol{N}^{(\mathrm{nc})}$, i.e.,

$$\Delta\mu_i = \mathrm{Im}\left\{\boldsymbol{r}_k^{(\mathrm{nc})^{\mathrm{T}}}\boldsymbol{W}^{(\mathrm{nc})}\boldsymbol{n}^{(\mathrm{nc})}\right\} + \mathcal{O}\{\Delta^2\}, \tag{13}$$

where $\boldsymbol{n}^{(\mathrm{nc})} = \mathrm{vec}\{\boldsymbol{N}^{(\mathrm{nc})}\} \in \mathbb{C}^{2MN\times 1}$,

$$\boldsymbol{r}_i^{(\mathrm{nc})} = \boldsymbol{q}_i^{(\mathrm{nc})} \otimes \left(\left[\left(\boldsymbol{J}_1^{(\mathrm{nc})}\boldsymbol{U}_{\mathrm{s}}^{(\mathrm{nc})}\right)^{+} \cdot \left(\boldsymbol{J}_2^{(\mathrm{nc})}/\lambda_i - \boldsymbol{J}_1^{(\mathrm{nc})}\right)\right]^{\mathrm{T}}\boldsymbol{p}_i^{(\mathrm{nc})}\right) \in \mathbb{C}^{2M\tilde{d}\times 1}, \tag{14}$$

and

$$\boldsymbol{W}^{(\mathrm{nc})} = \left(\boldsymbol{\Sigma}_{\mathrm{s}}^{(\mathrm{nc})^{-1}}\boldsymbol{V}_{\mathrm{s}}^{(\mathrm{nc})^{\mathrm{T}}}\right) \otimes \left(\boldsymbol{U}_{\mathrm{n}}^{(\mathrm{nc})}\boldsymbol{U}_{\mathrm{n}}^{(\mathrm{nc})^{\mathrm{H}}}\right) \in \mathbb{C}^{2M\tilde{d}\times 2MN}.$$

It is worth mentioning that (12) holds for all the $\tilde{d}$ virtual spatial frequencies. However, in order to compute the MSE, we need to distinguish between the strictly non-circular and the circular sources. This is due to the different processing for the circular sources, which includes the pairing of the two estimates for each circular source as well as their subsequent averaging. Note that the step of finding the correct pairing is not included in the presented performance analysis as this step never fails in the high effective SNR regime.

4.1. MSE of the Strictly Non-Circular Sources

The final MSE expression for the $d^{(\mathrm{nc})}$ strictly non-circular sources follows the results in [6]. Hence, the MSE for the k-th spatial frequency associated with the k-th non-circular source is given by

$$\begin{aligned}\mathbb{E}\left\{(\Delta\mu_k)^2\right\} = \frac{1}{2}\Big(&\boldsymbol{r}_k^{(\mathrm{nc})^{\mathrm{H}}}\boldsymbol{W}^{(\mathrm{nc})^{*}}\boldsymbol{R}_{\mathrm{nn}}^{(\mathrm{nc})^{\mathrm{T}}}\boldsymbol{W}^{(\mathrm{nc})^{\mathrm{T}}}\boldsymbol{r}_k^{(\mathrm{nc})}\\ &-\mathrm{Re}\left\{\boldsymbol{r}_k^{(\mathrm{nc})^{\mathrm{T}}}\boldsymbol{W}^{(\mathrm{nc})}\boldsymbol{C}_{\mathrm{nn}}^{(\mathrm{nc})^{\mathrm{T}}}\boldsymbol{W}^{(\mathrm{nc})^{\mathrm{T}}}\boldsymbol{r}_k^{(\mathrm{nc})}\right\}\Big) + \mathcal{O}\{\Delta^2\}.\end{aligned} \tag{15}$$

The expressions for the covariance matrix $\boldsymbol{R}_{\mathrm{nn}}^{(\mathrm{nc})} = \mathbb{E}\{\boldsymbol{n}^{(\mathrm{nc})}\boldsymbol{n}^{(\mathrm{nc})^{\mathrm{H}}}\}$ and the pseudo-covariance matrix $\boldsymbol{C}_{\mathrm{nn}}^{(\mathrm{nc})} = \mathbb{E}\{\boldsymbol{n}^{(\mathrm{nc})}\boldsymbol{n}^{(\mathrm{nc})^{\mathrm{T}}}\}$ were derived in [6] and can be expressed in terms of the SO statistics of the physical noise $\boldsymbol{n} = \mathrm{vec}\{\boldsymbol{N}\} \in \mathbb{C}^{MN\times 1}$. They are given by

$$\boldsymbol{R}_{\mathrm{nn}}^{(\mathrm{nc})} = \tilde{\boldsymbol{K}}\begin{bmatrix}\boldsymbol{R}_{\mathrm{nn}} & \boldsymbol{C}_{\mathrm{nn}}\\ \boldsymbol{C}_{\mathrm{nn}}^{*} & \boldsymbol{R}_{\mathrm{nn}}^{*}\end{bmatrix}\tilde{\boldsymbol{K}}^{\mathrm{T}},\ \ \boldsymbol{C}_{\mathrm{nn}}^{(\mathrm{nc})} = \tilde{\boldsymbol{K}}\begin{bmatrix}\boldsymbol{C}_{\mathrm{nn}} & \boldsymbol{R}_{\mathrm{nn}}\\ \boldsymbol{R}_{\mathrm{nn}}^{*} & \boldsymbol{C}_{\mathrm{nn}}^{*}\end{bmatrix}\tilde{\boldsymbol{K}}^{\mathrm{T}},$$

where $\boldsymbol{R}_{\mathrm{nn}} = \mathbb{E}\{\boldsymbol{n}\boldsymbol{n}^{\mathrm{H}}\}$, $\boldsymbol{C}_{\mathrm{nn}} = \mathbb{E}\{\boldsymbol{n}\boldsymbol{n}^{\mathrm{T}}\}$, and $\tilde{\boldsymbol{K}} = \boldsymbol{K}_{2M,N}^{\mathrm{T}} \cdot \mathrm{blkdiag}\{\boldsymbol{K}_{M,N}, \boldsymbol{K}_{M,N}(\boldsymbol{I}_N \otimes \boldsymbol{\Pi}_{M_{\mathrm{sub}}})\}$ with $\boldsymbol{K}_{M,N} \in \mathbb{R}^{MN\times MN}$ being the commutation matrix that satisfies $\boldsymbol{K}_{M,N} \cdot \mathrm{vec}\{\boldsymbol{A}\} = \mathrm{vec}\{\boldsymbol{A}^{\mathrm{T}}\}$ for arbitrary matrices $\boldsymbol{A} \in \mathbb{C}^{M\times N}$ [16].

4.2. MSE of the Circular Sources

For the MSE of the circular sources, we first take into account the averaging of the two correctly paired estimates for each circular source by computing

$$\begin{aligned}&\mathbb{E}\left\{\left(\frac{\hat{\mu}_\ell^{(1)} + \hat{\mu}_\ell^{(2)}}{2} - \mu_\ell\right)^2\right\} = \mathbb{E}\left\{\left(\frac{\Delta\hat{\mu}_\ell^{(1)} + \Delta\hat{\mu}_\ell^{(2)}}{2}\right)^2\right\}\\ &= \frac{1}{4}\left(\mathbb{E}\left\{(\Delta\hat{\mu}_\ell^{(1)})^2\right\} + \mathbb{E}\left\{(\Delta\hat{\mu}_\ell^{(2)})^2\right\} + 2\cdot\mathbb{E}\left\{\Delta\hat{\mu}_\ell^{(1)}\Delta\hat{\mu}_\ell^{(2)}\right\}\right).\end{aligned} \tag{16}$$

The first two terms of (16) can be calculated straightforwardly according to (15). The last term $\mathbb{E}\left\{\Delta\hat{\mu}_\ell^{(1)}\Delta\hat{\mu}_\ell^{(2)}\right\}$ represents the cross-correlation of the two estimates, which can be computed as follows:

Theorem 1. *Assuming that $\boldsymbol{N}^{(\mathrm{nc})}$ is zero-mean with finite SO moments, the first-order approximation of the cross-correlation between $\Delta\hat{\mu}_\ell^{(1)}$ and $\Delta\hat{\mu}_\ell^{(2)}$ is given by*

$$\begin{aligned}\mathbb{E}\left\{\Delta\hat{\mu}_\ell^{(1)}\Delta\hat{\mu}_\ell^{(2)}\right\} = \frac{1}{2}\Big(&\boldsymbol{r}_{\ell(1)}^{(\mathrm{nc})^{\mathrm{H}}}\boldsymbol{W}^{(\mathrm{nc})^{*}}\boldsymbol{R}_{\mathrm{nn}}^{(\mathrm{nc})^{\mathrm{T}}}\boldsymbol{W}^{(\mathrm{nc})^{\mathrm{T}}}\boldsymbol{r}_{\ell(2)}^{(\mathrm{nc})}\\ &-\mathrm{Re}\left\{\boldsymbol{r}_{\ell(1)}^{(\mathrm{nc})^{\mathrm{T}}}\boldsymbol{W}^{(\mathrm{nc})}\boldsymbol{C}_{\mathrm{nn}}^{(\mathrm{nc})^{\mathrm{T}}}\boldsymbol{W}^{(\mathrm{nc})^{\mathrm{T}}}\boldsymbol{r}_{\ell(2)}^{(\mathrm{nc})}\right\}\Big) + \mathcal{O}\{\Delta^2\},\end{aligned} \tag{17}$$

where $\boldsymbol{r}_{\ell(n)}^{(\mathrm{nc})}$, $n = 1, 2$ is given analogously to (13)*.*

Proof. To show this result, we first expand the two estimates $\Delta\hat{\mu}_\ell^{(n)} = \mathrm{Im}\left\{\boldsymbol{r}_{\ell(n)}^{(\mathrm{nc})^{\mathrm{T}}}\boldsymbol{W}^{(\mathrm{nc})}\boldsymbol{n}^{(\mathrm{nc})}\right\}$, $n = 1, 2$ by using (13). Then, we follow the steps of the derivation in [9] to obtain the desired result. □

Eventually, inserting (17) from Theorem 1 into (16), the MSE for the ℓ-th spatial frequency associated with the ℓ-th circular source can be expressed as

$$\begin{aligned}\mathbb{E}\left\{(\Delta\hat{\mu}_\ell)^2\right\} = \frac{1}{2}\Big(&\boldsymbol{z}_\ell^{\mathrm{H}}\boldsymbol{W}^{(\mathrm{nc})^{*}}\boldsymbol{R}_{\mathrm{nn}}^{(\mathrm{nc})^{\mathrm{T}}}\boldsymbol{W}^{(\mathrm{nc})^{\mathrm{T}}}\boldsymbol{z}_\ell\\ &-\mathrm{Re}\left\{\boldsymbol{z}_\ell^{\mathrm{T}}\boldsymbol{W}^{(\mathrm{nc})}\boldsymbol{C}_{\mathrm{nn}}^{(\mathrm{nc})^{\mathrm{T}}}\boldsymbol{W}^{(\mathrm{nc})^{\mathrm{T}}}\boldsymbol{z}_\ell\right\}\Big) + \mathcal{O}\{\Delta^2\},\end{aligned} \tag{18}$$

where $\boldsymbol{z}_\ell = \frac{1}{2}\left(\boldsymbol{r}_{\ell(1)}^{(\mathrm{nc})} + \boldsymbol{r}_{\ell(2)}^{(\mathrm{nc})}\right)$, which takes the averaging over the two estimates into account.

5. PERFORMANCE OF C-NC UNITARY ESPRIT

We have shown in [6] that NC Standard ESPRIT and NC Unitary ESPRIT designed for strictly non-circular sources enjoy the same analytical performance in the high effective SNR case. It was established that applying forward-backward averaging (FBA) to the augmented matrix $\boldsymbol{X}^{(\mathrm{nc})}$ does not improve the signal subspace estimate and that the real-valued transformation has no effect on the asymptotic performance in the high effective SNR regime. These properties still hold true for C-NC Standard ESPRIT and C-NC Unitary ESPRIT for the mixed signal case as the preprocessing for non-circular sources is conducted in the same way. Therefore, we can conclude that C-NC Standard ESPRIT and C-NC Unitary ESPRIT also perform identically in the high effective SNR.

6. SIMULATION RESULTS

In this section, we present numerical results to demonstrate the asymptotic behavior of the analytical performance assessment of C-NC Standard ESPRIT (C-NC SE) and C-NC Unitary ESPRIT (C-NC UE) algorithms designed for the mixed signal scenario. To this end, we compare the derived analytical ("ana") MSE expressions to the empirical ("emp") estimation errors of the algorithms obtained by averaging over Monte Carlo trials. The overall performance is benchmarked by the deterministic C-NC CRB (Det C-NC CRB) [15]. Additionally, we also include the ESPRIT-type methods (SE/UE) [17], [18] that do not exploit the NC structure of the strictly non-circular signals along with their analytical MSE

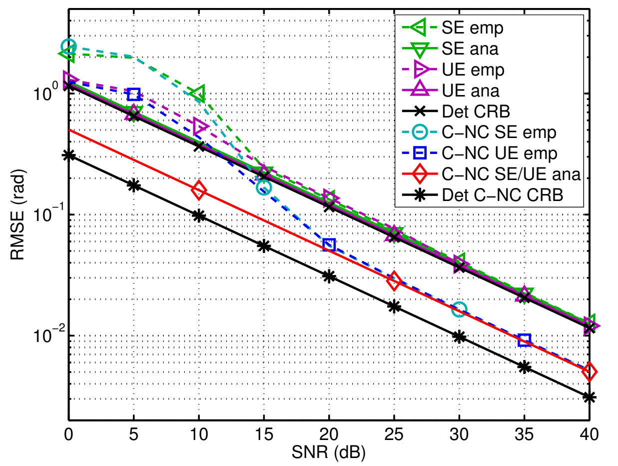

Fig. 1. RMSE versus SNR for $M = 8$, $N = 20$, $d^{(\mathrm{nc})} = 2$ sources at $\boldsymbol{\mu}^{(\mathrm{nc})} = [0.2, 1]$ with $\boldsymbol{\varphi}^{(\mathrm{nc})} = [0, \pi/2]$ and $d^{(\mathrm{c})} = 2$ sources at $\boldsymbol{\mu}^{(\mathrm{c})} = [0.5, 1.3]$.

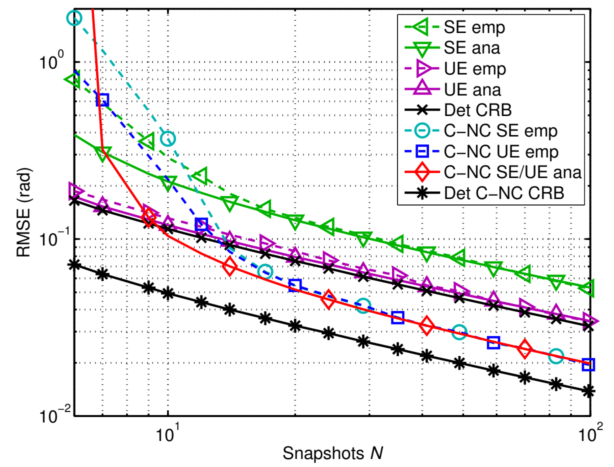

Fig. 2. RMSE versus snapshots N for $M = 8$, SNR = 25 dB, $d^{(\mathrm{nc})} = 2$ sources at $\boldsymbol{\mu}^{(\mathrm{nc})} = [0.2, 1]$ with $\boldsymbol{\varphi}^{(\mathrm{nc})} = [0, \pi/4]$, and $d^{(\mathrm{c})} = 2$ sources at $\boldsymbol{\mu}^{(\mathrm{c})} = [0.5, 1.3]$.

expressions [9]. All the ESPRIT-type algorithms use LS to solve the shift invariance equation. We employ a uniform linear array (ULA) composed of $M = 8$ isotropic sensors with $\delta = \lambda/2$ spacing. The phase reference of the array is located at its centroid. For the circular signals, the QPSK modulation scheme is used and the strictly non-circular signals are generated from a real-valued Gaussian distribution. Moreover, we assume the sensor noise to be circularly symmetric white Gaussian with variance σ_{n}^2. The curves are obtained by averaging over 5000 Monte Carlo trials.

In Fig. 1, we display the total RMSE over all sources as a function of the SNR. We assume a mixture of $d^{(\mathrm{nc})} = 2$ strictly non-circular sources at $\boldsymbol{\mu}^{(\mathrm{nc})} = [0.2, 1]$ with $\boldsymbol{\varphi}^{(\mathrm{nc})} = [0, \pi/2]$, and $d^{(\mathrm{c})} = 2$ circular sources at $\boldsymbol{\mu}^{(\mathrm{c})} = [0.5, 1.3]$. All the sources are uncorrelated and have unit power. The number of snapshots is $N = 20$. It is apparent from Fig. 1 that the analytical curves agree well with the empirical ones in the high SNR regime. Moreover, the asymptotic performance of C-NC SE and C-NC UE is identical at high SNRs. Nevertheless, C-NC UE should be preferred due to its lower computational complexity and better performance in the low SNR regime.

In Fig. 2, we use the same scenario but display the RMSE versus the number of snapshots N. The SNR is fixed at 25 dB. The rotation phases are given by $\boldsymbol{\varphi}^{(\mathrm{nc})} = [0, \pi/4]$ and the strictly non-circular sources have a pair-wise correlation of $\rho^{(\mathrm{nc})} = 0.9$. We can observe that the analytical curves and the empirical curves match well if at least $N = 20$ snapshots are available. Again, C-NC SE and C-NC UE perform asymptotically identical for a large sample size N.

In the third experiment, we consider a scenario with a varying number of strictly non-circular sources. We assume $N = 20$ snapshots and $d = 3$ uncorrelated sources at $\boldsymbol{\mu} = [0, 0.3, 0.8]$ with $\boldsymbol{\varphi} = [0, \pi/8, \pi/4]$. The curves labeled $d^{(\mathrm{nc})} = 1$ refer to the case, where the first source at $\mu^{(\mathrm{nc})} = 0$ is strictly non-circular and the remaining sources are circular, whereas for $d^{(\mathrm{nc})} = 2$, the two sources at $\boldsymbol{\mu}^{(\mathrm{nc})} = [0, 0.3]$ are strictly non-circular and the last one is circular. In Fig. 3, we display the RMSE of C-NC SE versus the SNR for the strictly non-circular source "(nc)" at $\mu_1 = 0$ and the circular source "(c)" at $\mu_3 = 0.8$ under the variation of $d^{(\mathrm{nc})}$. The strictly non-circular and the circular sources have the respective powers of $P^{(\mathrm{nc})} = 20$ and $P^{(\mathrm{c})} = 1$. As can be seen, the analytical curves verify the observation that an increasing number of strictly non-circular sources improves the estimation accuracy of the strictly non-circular sources as well as the circular sources.

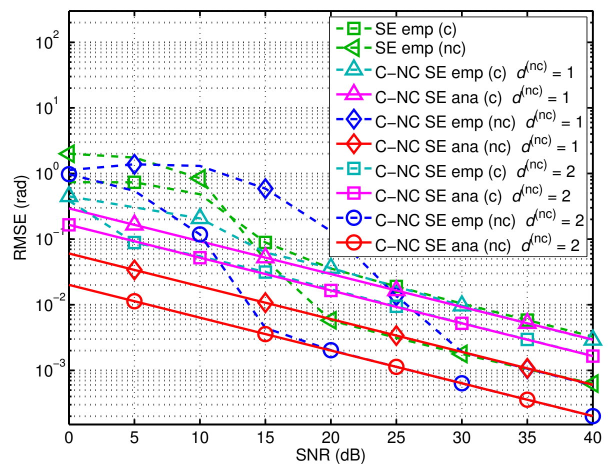

Fig. 3. RMSE versus SNR for the strictly non-circular "(nc)" source at $\mu_1 = 0$ and the circular "(c)" source at $\mu_3 = 0.8$ for $M = 8$, $N = 20$, $P^{(\mathrm{nc})} = 20$, and $P^{(\mathrm{c})} = 1$ with varying $d^{(\mathrm{nc})}$.

7. CONCLUSION

In this paper, we have presented a first-order performance assessment of the recently developed C-NC Standard ESPRIT and C-NC Unitary ESPRIT algorithms for coexisting circular and strictly non-circular sources. Specifically, we have derived closed-form MSE expressions that are asymptotic in the effective SNR, i.e., the approximations become exact for either high SNRs or a large sample size. Moreover, apart from a zero mean and finite SO moments, no further assumptions on the noise statistics are required. We have shown that both algorithms perform identical in the high effective SNR and that the analytical results verify the previously observed property that the presence of strictly non-circular sources improves the estimation accuracy of the circular sources.

8. REFERENCES

[1] P. J. Schreier and L. L. Scharf, *Statistical Signal Processing of Complex-Valued Data: The Theory of Improper and Noncircular Signals*, Cambridge, U.K.: Cambridge Univ. Press, 2010.

[2] H. Abeida and J. P. Delmas, "MUSIC-like estimation of direction of arrival for noncircular sources," *IEEE Transactions on Signal Processing*, vol. 54, no. 7, pp. 2678-2690, July 2006.

[3] P. Chargé, Y. Wang, and J. Saillard, "A non-circular sources direction finding method using polynomial rooting," *Signal Processing*, vol. 81, no. 8, pp. 1765-1770, Aug. 2001.

[4] A. Zoubir, P. Chargé, and Y. Wang, "Non circular sources localization with ESPRIT," in *Proc. European Conference on Wireless Technology (ECWT 2003)*, Munich, Germany, Oct. 2003.

[5] M. Haardt and F. Roemer, "Enhancements of Unitary ESPRIT for non-circular sources," in *Proc. IEEE Int. Conf. on Acoust., Speech, and Sig. Proc. (ICASSP)*, Montreal, Canada, May 2004.

[6] J. Steinwandt, F. Roemer, M. Haardt, and G. Del Galdo, "R-dimensional ESPRIT-type algorithms for strictly second-order non-circular sources and their performance analysis," *IEEE Transactions on Signal Processing*, vol. 62, no. 18, pp. 4824-4838, Sep. 15, 2014.

[7] H. Abeida and J. P. Delmas, "Statistical performance of MUSIC-like algorithms in resolving noncircular sources," *IEEE Transactions on Signal Processing*, vol. 56, no. 9, pp. 4317-4329, Sep. 2008.

[8] F. Li, H. Liu, and R. J. Vaccaro, "Performance analysis for DOA estimation algorithms: Unification, simplifications, and observations," *IEEE Transactions on Aerospace and Electronic Systems*, vol. 29, no. 4, pp. 1170-1184, Oct. 1993.

[9] F. Roemer, M. Haardt, and G. Del Galdo, "Analytical performance assessment of multi-dimensional matrix- and tensor-based ESPRIT-type algorithms," *IEEE Transactions on Signal Processing*, vol. 62, pp. 2611–2625, May 2014.

[10] F. Gao, A. Nallanathan, and Y. Wang, "Improved MUSIC under the coexistence of both circular and noncircular sources," *IEEE Transactions on Signal Processing*, vol. 56, no. 7, pp. 3033-3038, July 2008.

[11] A. Liu, G. Liao, Q. Xu, and C. Zeng, "A circularity-based DOA estimation method under coexistence of noncircular and circular signals," in *Proc. IEEE Int. Conf. on Acoust., Speech, and Sig. Proc. (ICASSP)*, Kyoto, Japan, March 2012.

[12] A. Ferreol and P. Chevalier, "Higher order direction finding for arbitrary noncircular sources: The NC-2q-MUSIC algorithm," in *Proc. of the European Signal Processing Conference (EUSIPCO)*, Aalborg, Denmark, Aug. 2010.

[13] J. Steinwandt, F. Roemer, and M. Haardt, "ESPRIT-type algorithms for a received mixture of circular and strictly non-circular signals," in *Proc. IEEE Int. Conference on Acoustics, Speech, and Signal Processing (ICASSP)*, Brisbane, Australia, Apr. 2015.

[14] J. Steinwandt, F. Roemer, M. Haardt, and G. Del Galdo, "Deterministic Cramér-Rao bound for strictly non-circular sources and analytical analysis of the achievable gains" arXiv:1504.00203, Apr. 2015.

[15] J. Steinwandt, F. Roemer, and M. Haardt, "Deterministic Cramér-Rao bound for a mixture of circular and strictly non-circular signals," in *Proc. International Symposium on Wireless Communications Systems (ISWCS)*, Brussels, Belgium, Aug. 2015.

[16] J. R. Magnus and H. Neudecker, *Matrix differential calculus with applications in statistics and econometrics*, John Wiley and Sons, 1995.

[17] R. H. Roy and T. Kailath, "ESPRIT-estimation of signal parameters via rotational invariance techniques," *IEEE Transactions on Acoustics, Speech, and Signal Processing*, vol. 37, no. 7, pp. 984-995, July 1989.

[18] M. Haardt and J. A. Nossek, "Unitary ESPRIT: How to obtain increased estimation accuracy with a reduced computational burden," *IEEE Transactions on Signal Processing*, vol. 43, no. 5, pp. 1232-1242, May 1995.